Available online at www.sciencedirect.com
SCIENCE DIRECT
Polymer Testing 25 (2006) 443–451
POLYMER TESTING
www.elsevier.com/locate/polytest

Test Method

Atomic force acoustic microscopy analysis of epoxy–silica nanocomposites

Michele Preghenella*, Alessandro Pegoretti, Claudio Migliaresi

Department of Materials Engineering and Industrial Technologies and INSTM Research Unit, University of Trento, via Mesiano, 77, 38050 Trento, Italy

Received 6 December 2005; accepted 16 January 2006

Abstract

A DGEBA-based epoxy matrix was loaded with 10, 20 and 30 phr of fumed silica particles. Single edge notched bend (SENB) specimens were prepared and deformed to failure in three-point bending configuration. Their fracture surfaces were examined by atomic force acoustic microscopy (AFaM) in order to obtain information about the local elastic modulus of the surface at high spatial resolution. The collected information was correlated to the bulk thermo-mechanical properties of the composites. In particular, the decrease in thermo-mechanical properties like tensile modulus, yield strength, stress at break and glass transition temperature, observed for samples filled with 10 and 20 phr with respect to the unfilled matrix was found to correspond to highly heterogeneous fracture surfaces presenting a broad distribution of elastic modulus values. The AFaM data were interpreted as representative of different degrees of filler exposure on fracture surfaces and also of localized cavitation effects involved in crack propagation, both phenomena accounting for the effective plasticizing effect macroscopically observed at silica amounts of 10 and 20 phr. A substantial reduction in the exposure probability of silica particles on fracture surfaces was found for the sample filled with 30 phr of silica, which also displayed an improvement of the mechanical and thermal properties. This latter evidence was tentatively explained by supposing a physical immobilization of polymer chains at the polymer-matrix interface.

Keywords: Elastic modulus; Epoxy; Silica; Nanocomposites; Atomic force microscopy; Acoustic modality

1. Introduction

In recent years, great attention has been focused on polymeric nanocomposites, especially those obtained from layered silicates [1,2] dispersed in thermoplastic and thermosetting matrices. If properly dispersed, these fillers can substantially improve the properties of the resulting nanocomposites with respect to conventional microcomposites loaded with the same amount of filler. In fact, the properties of the polymeric matrices can be substantially altered by the interactions with a nano-filler. The main reason for this behavior has been identified in the much higher interfacial area between matrix and filler in nanocomposites than in conventional microcomposites [1,2]. As a consequence, the macroscopic behavior of the nanocomposites cannot be accurately predicted by the rules proposed for microcomposites [3] and sometimes unexpected

*Corresponding author. Tel.: +39 0461 882411; fax: +39 0461 881977.
E-mail address: michele.preghenella@ing.unitn.it (M. Preghenella).

0142-9418/$ - see front matter © 2006 Elsevier Ltd. All rights reserved.
doi:10.1016/j.polymertesting.2006.01.009

effects can be observed in thermal [4–6] and mechanical properties.

The availability of a wide range of operative techniques in atomic force microscopy (AFM) [7] allows one to carefully control the degree of sample-probe interaction while preserving sample integrity. This is one of the reasons why AFM has been widely used to analyze non-conductive samples, especially in those cases where any substrate preparation could potentially alter the observed microstructure or when the required resolution level was critical [8–10]. Moreover, the analysis of direct contact force with the substrate allows one to obtain information on the mechanical response of highly localized portions of a given microstructure. In this way, it is possible to have almost direct access to microscopic quantities otherwise only derivable from theoretical, or even phenomenological, models [11–14] based on macroscopic average values.

In the present work we focus our attention on the use of atomic force acoustic microscopy (AFaM) for the analysis of fracture surfaces of epoxy-based silica-nanocomposites in an attempt to correlate their sub-micrometric structure, as revealed by the distribution of local elastic modulus, to their macroscopic thermo-mechanical behavior. That behavior has been extensively investigated by this research group and described in a companion paper [15]. Unlike previous works concerning polymeric composites, which emphasized the imaging capabilities of the AFM techniques, we focused our attention on the possibility of gaining numerical information characterizing the physical appearance of the fractured surfaces, analyzed to correlate them with the bulk thermo-mechanical properties already measured. The acoustic mode (AFaM) was selected to exploit the higher stiffness which is exhibited by a viscoelastic material at the ultrasonic frequencies used to perform measurements, since previous works reported on the difficulties of determining elastic characteristic in polymeric nanocomposites by "static" force-distance spectroscopy [16]. Moreover, the choice of AFaM technique to investigate the fracture surface was prompted by the high spatial resolution required to recognize structural heterogeneity on sub-micrometric scale in nanocomposites. In fact, scanning electron microscopy techniques like backscattered electrons (BSE) imaging or energy dispersion X-Ray spectroscopy (EDXS) are sensitive to compositional differences but lack the required lateral and in depth resolutions. This can be easily recognized just considering that typical penetration depth of BSE analysis is about 200 nm and that one of EDXS is as high as 500 nm (depending on sample and operative conditions), while AFaM spectroscopy sampling depth in our case was estimated to be less than 25 nm.

2. Experimental section

The selected epoxy matrix was a commercial bicomponent system (EC57/K63), supplied by Camattini S.p.A. (Collecchio, Parma, Italy), consisting of a DGEBA-based low molecular weight epoxy resin (EC57: epoxy-equivalent 172–182 g/eq) and a polyamide–amine curing agent (K63: 88–91 g/eq). The filler was the Cab-O-Sil M5 fumed silica, supplied by Cabot GmbH (Hanau, Germany), consisting of nanometric particles of untreated pure amorphous silica with nominal surface area of about 200 m^2/g. Composite samples conforming to UNI EN ISO 527 type 1BA dumb-bell geometry were prepared with filler loadings of 10, 20 and 30 phr (corresponding to 6.3, 11.8 and 16.7 percent by weight and to 3.3, 6.4 and 9.2 percent by volume, respectively) by a solvent assisted dispersion procedure accurately described in a companion paper [15]. Samples for three-point bending tests were machined from the central part of dumb-bell test pieces to obtain single-edge notched bend samples (SENB) conforming to the ISO 13586-1 standard test method for the determination of the plane-strain fracture toughness and strain energy release rate of plastic materials. Tests were performed by a 4052 Instron tensile testing machine at a cross-head speed of 1 mm/min. AFM and AFaM analyses were performed on the fracture surfaces of SENB specimens using an Nt-Mdt Solver P47H scanning probe microscope equipped with a piezoelectric sample holder. Nt-Mdt NSG silicon gold tips with nominally 5.5 N/m elastic constant and 150 kHz first resonance frequency were utilized. Calibrations were performed on an electronic grade (1 0 0) silicon wafer surface ($E = 130$ GPa, $\nu = 0.181$), previously cleaned from organic residues with chromic mixture and treated in HF (80% aq) for 30 min in an ultrasonic bath (Branson 2510, 47 kHz, 125 W) to remove the surface oxidized layer. Representative areas on the fracture surfaces of the composites and the unfilled matrix were selected to acquire topographic images (in contact and tapping mode) and amplitude-oscillation images (in tapping mode). Since all the samples were found to be homogeneous at a micrometric scale when observed

in the aforementioned modes, the more time-consuming AFaM spectroscopic analyses were performed on smaller areas (of $1\,\mu m \times 1\,\mu m$), randomly chosen on the surface. Each of these areas were scanned on a grid of 225 equally spaced points, where the contact resonance frequency was measured and the local elastic modulus was assessed relying on the theoretical basis briefly reported in the following section. In order to generate statistically significant results, for each sample a number of points in the range from 1000 to 2000 was recorded and analyzed, depending on sample heterogeneity.

3. Theoretical basis

The purpose of this section is to briefly recall the principle of acoustic spectroscopy measurements performed by the atomic force microscope, and to point out the theoretical background and the fundamental assumptions behind the modeling of the tip-sample contact which allows one to estimate the local elastic modulus from the resonance frequency data. An exhaustive description of the all the different imaging modes in AFM was given by Wiesendanger [7].

A schematic representation of the so-called acoustic modality of AFM is given in Fig. 1. The sample is in contact with an ultrasonic transducer which can be excited at a given frequency by means of a signal generator. The vibrations, transferred to the cantilever through the tip, produce flexural oscillations that are detected by means of a laser-photodiode optical system. Both amplitude and average position of the oscillating cantilever can be measured simultaneously. After a topographic image has been acquired (see Fig. 2), the spectroscopic mode can be used to identify the resonance frequencies at several points on the surface. As represented in Fig. 3, the resonance frequency can be identified as the frequency that induces the maximum amplitude in the cantilever oscillations.

The mathematical approach for modeling the probe oscillations relies on the Saint Venant's theory for a linear elastic cantilever [17] and the Hertzian contact tip-sample interaction model [12]. The cantilever is hence assumed to be a linear elastic solid whose characteristic equation for free oscillation can be written as:

$$\cosh(k_n L)\ \cos(k_n L) + 1 = 0 \tag{1}$$

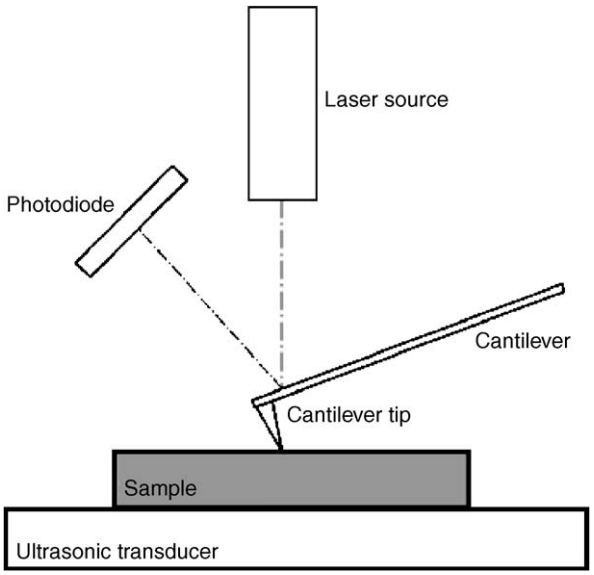

Fig. 1. Operating principle of an atomic force microscope in acoustic mode (AFaM).

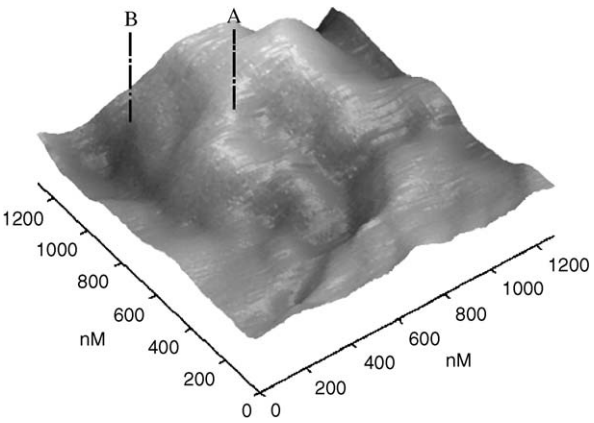

Fig. 2. AFM topography of a composite sample filled with 20 phr fumed silica. Points A and B are marker for the acoustic spectroscopy showed in the next figure.

and

$$k_n^2 = f\sqrt{4\pi^2\,\frac{12\rho}{t^2 E}} = f\,c_B^2, \tag{2}$$

where L is the length of the cantilever, k_n is wave number of the stationary wave propagating in the cantilever; f is the frequency of the vibrations; ρ and E the density and the Young modulus of the material, respectively; t the thickness of the beam; c_B a constant summarizing all the elastic characteristics of the tip. By solving the characteristic Eq. (1) for the free oscillation modes k_n and measuring the

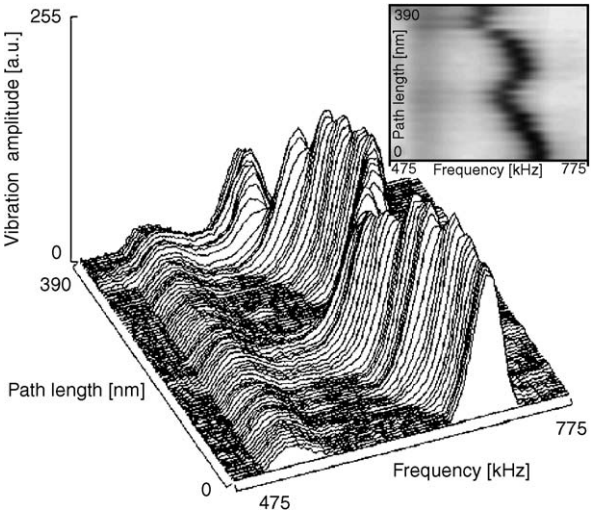

Fig. 3. Acoustic spectroscopy showing the frequency variations of the cantilever vibration amplitude along the surface path from point A to point B of Fig. 2. Resonance frequency is about 720 kHz in point A and 675 kHz in point B.

corresponding resonance frequency f, the dynamic constant c_B of the tip can be obtained. It should be noted that any resonance mode can be used in principle to determine the c_B value but the more intense one should be preferred.

The contact of the cantilever tip with the substrate is assumed to be linear elastic. Under these hypotheses, the characteristic equations describing the flexural resonance conditions of the system take the following form [12]:

$$\frac{k*}{k_C}\,[-(\cosh k_n L_1 \sin k_n L_1 - \sinh k_n L_1 \cos k_n L_1) \times(1+\cos k_n L' \cosh k_n L') + (\cosh k_n L' \sin k_n L' - \sinh k_n L' \cos k_n L') \times(1-\cos k_n L_1 \cosh k_n L_1)] = 2\frac{(k_n L_1)^3}{3}(1+\cos k_n L \cosh k_n L), \quad (3)$$

where k_n is the wave number of the flexural vibration, k_C is the elastic constant of the cantilever and k^* is the elastic constant of the spring by which the tip-substrate interactions are modeled. As it is shown in Fig. 4, L_1 and L' are the distances locating the tip position from the cantilever base and the free edge, respectively.

After the Hertzian contact model, the k^* elastic constant is related to the geometry of the contact and the elastic characteristic of the two contacting

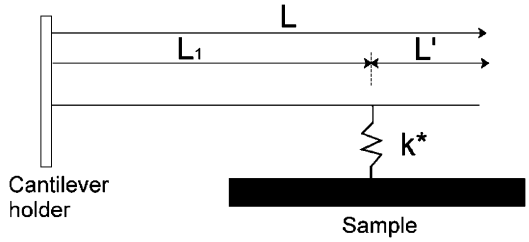

Fig. 4. Linear elastic contact model for tip-sample interactions.

bodies by the following equations [12]:

$$k^* = \sqrt[3]{6(E^*)^2 R^* F_N}, \quad (4)$$

$$\frac{1}{E^*} = \frac{1-\nu_1}{E_1} + \frac{1-\nu_2}{E_2}, \quad (5)$$

$$\frac{1}{R^*} = \frac{1}{R_1} + \frac{1}{R_2}, \quad (6)$$

where E^* is the equivalent contact modulus, E_1 and E_2 the elastic moduli of the two bodies, ν_1 and ν_2 the Poisson's ratios of the two bodies, F_N is the normal force involved in the contact and R^* is the equivalent contact radius, R_1 and R_2 being the radii of curvature of the two contacting bodies in the contact point, viz. the tip and the surface.

If any resonant frequency of the cantilever in contact with the substrate under the load F_N is measured, Eqs. (2) and (3) can be solved directly for k^* and then E^* can be quantified from Eqs. (4)–(6). For this purpose, the knowledge of the geometric characteristics of the cantilever is required, in particular the tip radius R. During the calibration procedure the cantilever resonance frequency is measured on a flat substrate whose elastic modulus and Poisson's ratio are known, thus allowing the radius R of the tip to be estimated. In accordance with Rabe et al. [12], we used silicon (1 0 0) as a reference material with $E = 130$ GPa and $\nu = 0.181$. The estimates of the tip curvature radius R were made for a new cantilever before scanning the samples and after a given number of scans: the values were found to grow, probably because of tip fouling due to the polymeric substrate, and an average value of 37 ± 10 nm was used throughout the modulus calculations. During the measurement operations, the Eqs. (2)–(6) were solved for E^* and thus for the elastic modulus of the substrate in the approximation of $R^* = R_1$. The influence of curvature radius R_2 of the sample surface at the contact point was disregarded because topographic analysis

revealed that the values of R_2 always exceeded 120 nm. For the average tip radius R_1 of 37 nm, the approximation $R^* = R_1$ corresponds to an error of about 15% in the estimate of E^* (either positive or negative depending on the surface curvature sign) which in turn brought about an error of 16–22% in the estimate of the substrate modulus E_2 over the explored frequency range. These values are actually lower than the uncertainties due to the variation in curvature tip radius as shown in Fig. 5, the latter being greater at higher resonance frequencies.

In the calculations of E_2, the value of the Poisson's ratio of the substrate v_2 was approximated by the value of 0.3 since the experiments were performed at room temperature (25 °C ca) and vibration frequencies were high enough to fall in the glassy state region of the viscoelastic composites, as predicted by dynamic mechanical tests via the time–temperature-superimposition principle (TTSP) [15].

According to the Hertzian contact model, when contacting the sample the tip develops a stress field whose lateral dimensions and penetration depth under the surface are related to the following scale parameter:

$$a = \sqrt[3]{\frac{3F_N R^*}{4E^*}}. \quad (7)$$

The parameter a becomes significant in defining the sampling dimensions of the spectroscopic analysis because only the material experiencing the stress field generated by the tip takes part in the elastic reaction modeled by the spring k^*. The estimated value for E of the substrate actually corresponds to an average on the stressed volume. The dependence of the characteristic sampling dimension (a) on the resonance frequency is shown in Fig. 6. The stress field intensity, represented by the ratio of von Mises equivalent stress to maximum contact pressure developed in a sphere–plane contact, is reduced to less than 10% of its maximum at a penetration depth of $3a$ under the surface and to less than 5% at a lateral displacement of $2a$ from the contact point [18,19]. Consequently, we can consider the E value obtained in a given point as a mean value representative of the material located inside the aforementioned geometrical boundaries which, for the samples analyzed, can be estimated to be always less than 25 nm apart from the contact point, since the maximum a values obtained were less than 8 nm as measured in correspondence to the lowest detected contact resonance frequency.

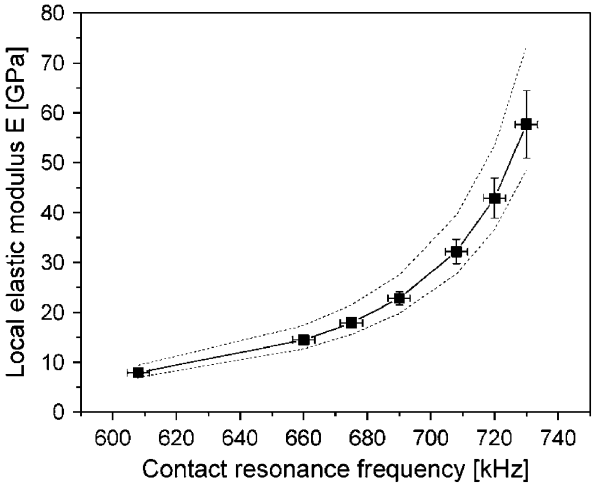

Fig. 5. Variation of the local elastic modulus with the contact resonance frequency calculated for a mean tip radius of 37 nm (scattered dots connected by solid line) and for tip radius variation between 27 and 47 nm (dashed lines).

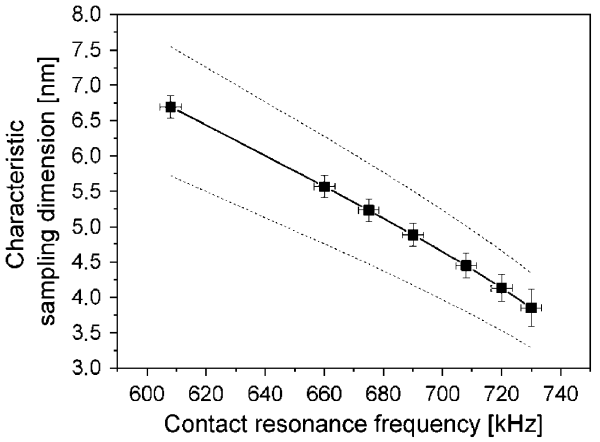

Fig. 6. Variation of the characteristic sampling dimension with the contact resonance frequency calculated for a mean tip radius of 37 nm (scattered dots connected by solid line) and for tip radius variation between 27 and 47 nm (dashed lines).

4. Results and discussion

An extended investigation of the thermo-mechanical properties of the selected materials is presented and discussed in a companion paper by this research group [15]. Some of the thermo-mechanical properties of the silica–epoxy nanocomposites are summarized in Table 1. It is interesting to observe that a decrease in thermo-mechanical properties, such as glass transition temperature, dynamic storage modulus, Young's modulus, yield strength and stress at

Table 1
Thermo-mechanical properties of silica epoxy-composites [15]

Silica content (phr)	Elastic modulus (MPa)	Yield strength (MPa)	Stress at break (MPa)	Tg[a] (°C)
0	2260±71	35.3±0.8	30.2±0.9	67±1
10	1500±120	17.8±0.8	19.7±0.3	57±1
20	1900±150	21.3±0.6	23.8±1.0	53±2
30	2800±240	25±0.6	24.9±0.7	55±1

[a]Glass transition temperature as peak temperature of dynamic loss modulus at 1 Hz.

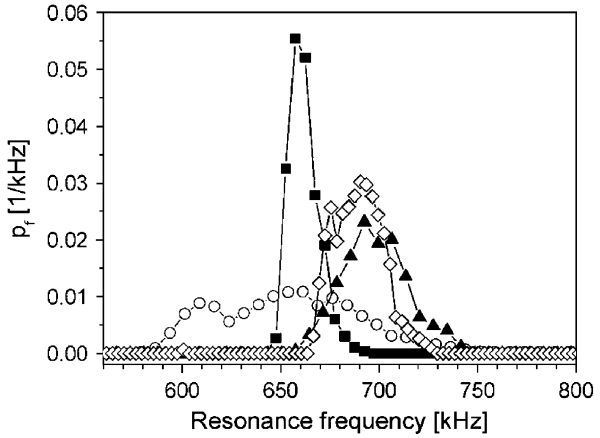

Fig. 7. Probability distribution function p_f [kHz^{-1}] for the contact resonance frequencies measured on the fracture surfaces. Silica content in phr: 0 (■), 10 (○), 20 (▲), 30 (◇).

break occurs for samples filled with 10 and 20 phr, while a trend inversion can be observed for samples with a silica content of 30 phr.

AFaM acoustic spectroscopy was used to analyze the fracture surface of SENB specimens, as described in the previous section. The collected resonance frequencies allowed us to generate the statistical distributions presented in Fig. 7. The function p_f is the probability distribution function of the resonance frequencies measured on the fracture surfaces. The integral of p_f over a frequency interval represents the cumulative probability for resonance frequencies to occur inside that interval, and it also represents the fraction of the surface exhibiting contact resonance frequencies values inside that interval. The data were properly normalized in order to yield a cumulative probability value equal to 1 over the entire explored frequency range. Taking into account the relationship between the resonance frequency and the local elastic modulus,

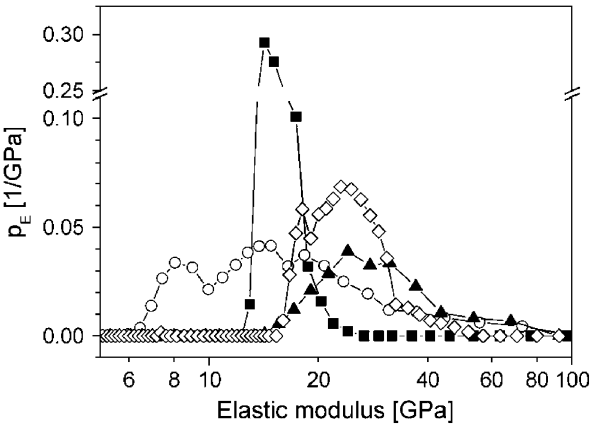

Fig. 8. Probability distribution function p_E [GPa^{-1}] for the local elastic modulus measured on the fracture surfaces. Silica content in phr: 0 (■), 10 (○), 20 (▲), 30 (◇).

as stated in the theoretical basis section, the distributions in the frequency domain p_f were replotted in the elastic moduli domain p_E as reported in Fig. 8.

The fractured surface of the unfilled sample exhibited a sharp p_E distribution, while for the filled samples much broader distributions were found, indicating the presence of a more heterogeneous structure. As expected, all the samples filled with silica nanoparticles showed high modulus spectral components in their p_E distributions accounting for the probability to find some silica particles almost completely exposed on the fracture surface. In fact, the highest value of elastic modulus detected on the surfaces is around 70 GPa, very close to the elastic modulus of amorphous silica [20]. However, in the case of 10 phr fumed silica nanocomposites a significant portion of the surface showed elastic modulus values lower than those of the unfilled matrix. This observation is in agreement with the macroscopic behavior of this composite. In fact, as reported in Table 1, the tensile tests evidenced Young's modulus, yield strength and stress at break values much lower than those measured on all the other compositions.

The highest values of local elastic modulus were found in the sample filled with a silica content of 20 phr, and appeared to correspond to topographic reliefs as shown in Figs. 2 and 3. On the contrary, no direct relation was found between topography and local stiffness where these latter values were significantly lower than those of the unfilled matrix, as in the case of 10 phr filled samples. Figs. 9 and 10 show a representative topographic path and the

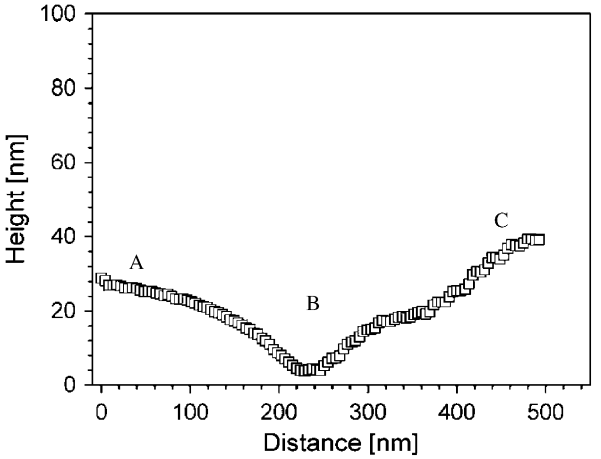

Fig. 9. Example of topographic profile on the fracture surface of a composite (10 phr filled sample). The vertical scale is enlarged to appreciate the topographic relief; roughness on sub-micrometric scale was found to be generally low.

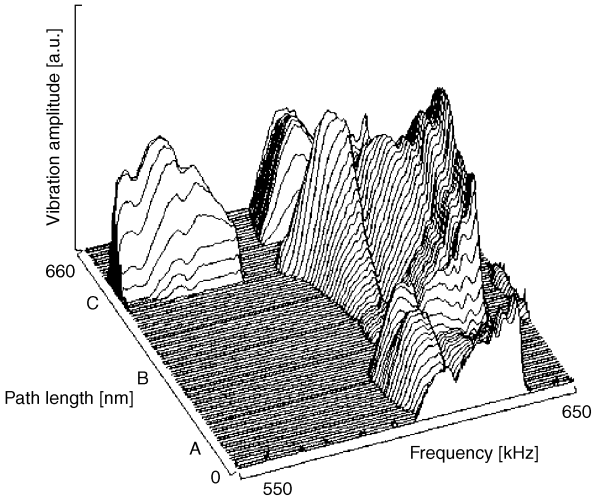

Fig. 10. AFaM spectroscopy along the surface path represented in Fig. 9.

corresponding spectroscopic profile acquired on the fracture surface of 10 phr silica nanocomposites. Comparable resonance values were measured at points A and B (marked in Figs. 9 and 10), regardless of their topographic location. Point C, showing resonance frequency as low as 570 kHz, was found to exhibit an anomalous sticking behavior as represented in Fig. 11 where force-distance spectroscopy curves [7] acquired at points B and C are shown. The cantilever deflection current in Fig. 11 represents the current intensity measured by the laser-photodiode system (see Fig. 1) as a result of the cantilever deflection while in contact with the substrate, and is proportional to

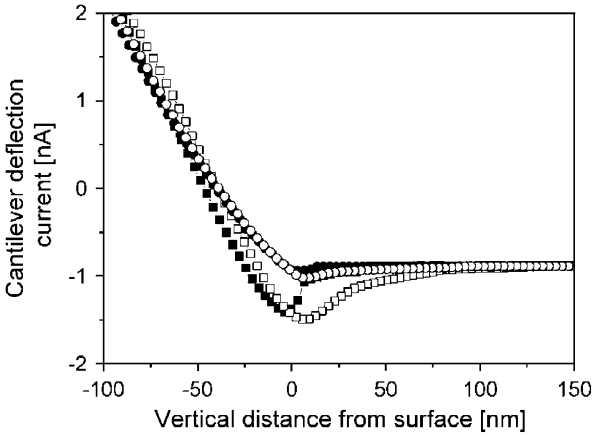

Fig. 11. Force-distance spectroscopy acquired in points B and C marked in Figs. 9 and 10. Point B (●) approaching and (○) detaching from the surface. Point C (■) approaching and (□) detaching from the surface.

Table 2
Integrated values of the probability distributions p_E of local elastic moduli

Silica content (phr)	Integrated p_E for $E > 30$ GPa
0	0
10	0.37
20	0.55
30	0.25

the contact force. The vertical distance is measured on the abscissa as positive from the surface. Point C showed a substantially higher adhesion force toward the probe tip as revealed by the pronounced negative minima of force-distance plots in detaching the tip from the sample.

By comparing the obtained p_E distributions at different filler content, we observed a reduced probability of finding local elastic moduli higher than 30 GPa in the case of 30 phr filled samples compared to 10 and 20 phr filled ones, as shown in Fig. 8 and Table 2.

The results obtained for the distributions of elastic stiffness and their relative levels on the fracture surface can be related to the bulk thermo-mechanical data partially reported in Table 1 and more extensively in Ref. [15]. The heterogeneity of fracture surfaces evidenced by AFaM correlated fairly well with mechanical tests, showing an enhanced plastic behavior in silica-filled composites with respect to the unfilled matrix. The lowest local elastic modulus values observed for 10 phr silica

nanocomposites were supposed to be related to localized cavitations phenomena occurring in front of the propagating crack. On the other hand, the highest values observed for 20 phr silica-filled samples were attributed to silica particles almost completely exposed on the fracture surface because of the poor interfacial bond strength between filler and matrix. This effect could probably be induced by a reduction in matrix crosslink-density near the silica particles, which are thought to hinder the molecular mobility of reactive groups involved in the curing reaction. This interpretation was supported by the reduction of glass transition temperatures (observed both in DSC and DMTA) and an increase in the damping capacity in nanocomposites with respect to unfilled matrix [15]. However, no direct proof was obtained of cavitation occurring while fracturing the samples until the local elastic stiffness was measured by AFaM. Density measurements were unable to detect such localized phenomena, nor did SEM images succeed at this because of the highly deformed appearance of the composites surfaces by themselves.

In the case of 30 phr filled sample, the reduction of p_E distribution values for modulus values higher than 30 GPa could be related to stronger interactions between filler and matrix, since the fracture front propagated across the sample ligament leaving a noticeably lower amount of silica particles almost exposed. This interpretation is coherent with DSC and fracture toughness data [15] and also with DMTA loss factor spectra (both in the temperature and in the frequency domains) that indicated the presence of strong polymer–filler interactions limiting the matrix molecular mobility.

Lastly, it is worth commenting about the values of local elastic modulus measured on the fracture surface of the unfilled samples. The peak resonance frequency was detected at 658 kHz, corresponding to a local elastic modulus of about 14 GPa; by comparison the value of the dynamic storage modulus predicted by means of the TTSP from dynamic mechanical data previously reported was about 1.7 GPa at the same frequency [15]. The quantities were different by a factor of almost 8.5, which could be ascribed to the shortcoming of the simple linear elastic Hertzian contact model used to calculate the elastic modulus values from the contact resonance frequency. On the other hand, the estimate of the E' modulus by TTSP could be affected itself by uncertainty since no DMTA tests were actually performed on the samples at such a high frequency. Finally, one could also suppose that the material facing the fractured surfaces measured by AFM could have an higher elastic modulus due the its highly deformed state, as evidenced by fracture toughness test data previously reported [15]. Actually, the maximum elastic modulus values measured by AFM on the fracture surface of 20 phr filled samples was about 68 GPa, which agreed very well with the elastic modulus of silica particles. In this case, concurrent SEM observations confirmed that the filler was partially exposed on the fractured surface [15]. Apart from the arguments about the accuracy, the AFaM technique succeeded in detecting the heterogeneity of the composite fractured surface, allowing us to obtain a quantitative estimate of the surface stiffness by the distribution probability of the contact resonance frequencies. The information resulted in a good correlation with the observed trend in thermo-mechanical properties measured by conventional techniques [15].

5. Conclusions

Atomic force acoustic microscopy was used to analyze the microstructural heterogeneity on the fracture surface of silica-filled epoxy nanocomposites. The distributions of contact resonance frequency were obtained and, after proper calibration, these data were converted into local elastic modulus distributions. The results were tentatively related to the bulk thermo-mechanical behavior. In particular, the decrease in thermo-mechanical properties such as glass transition temperature and dynamic storage modulus for 10 and 20 phr filled samples was found to correspond to highly heterogeneous fracture surfaces presenting a wide range of elastic stiffness values. These heterogeneities were interpreted as representative of different degrees of filler exposure on the fracture surfaces and also of localized cavitation effects involved in crack propagation, both phenomena accounting for the effective plasticizing effect induced by silica amounts of 10 and 20 phr.

A substantial reduction in the exposure probability of silica particles on fracture surfaces was found for 30 phr filled samples corresponding to an improvement of the observed mechanical and dynamic–mechanical properties. This latter feature was tentatively attributed to the physical immobilization of polymer chains at the polymer–matrix interface.

Acknowledgment

This work was carried out with the financial support of the ''Ministero dell'Istruzione dell'Università e della Ricerca'' (MIUR—Italy), PRIN 2003 (Grant no. 2003093440_002).

References

[1] M. Alexandre, P. Dubois, Polymer-layered silicate nanocomposites: preparation, properties and uses of a new class of materials, Mater. Sci. Eng. 28 (2000) 1–63.
[2] T. Lan, T.J. Pinnavaia, Clay-reinforced epoxy nanocomposites, Chem. Mater. 6 (1994) 2216–2219.
[3] L.E. Nielsen, J. Compos. Mater. 1 (1967) 100–119.
[4] V. Arrighi, I.J. McEwen, H. Quian, M.B. Serraro Prieto, The glass transition and interfacial layer in styrene–butadiene rubber containing silica nanofiller, Polymer 44 (2003) 6259–6266.
[5] Y. Huang, S. Jiang, L. Wu, Y. Hua, Characterization of LLDPE/nano-SiO2 composites by solid-state dynamic mechanical spectroscopy, Polym. Test. 23 (2004) 9–15.
[6] H. Zhang, B. Wang, H. Li, Y. Jiang, J. Wang, Synthesis and characterization of nanocomposites of silicon dioxide and polyurethane and epoxy resin interpenetrating network, Polym. Int. 52 (2003) 1493–1497.
[7] R. Wiesendanger, Scanning Probe Microscopy and Spectroscopy, Cambridge University Press, Cambridge, 1994.
[8] S. Ray, A.K. Bhowmick, Atomic force microscopy study on morphology and distribution of surface modified fumed silica and clay fillers in an ethylene–octene copolymer rubber, Rubber Chem. Technol. 76 (2003) 1091–1105.
[9] G. Merle, A.C. Grillet, J. Allemand, D. Leseur, Quantitative analysis of surface morphology: characterization of polypyrrole films aging, Polym. Test. 18 (1999) 217–229.
[10] E. Radovanovic, E. Carone Jr, M.C. Goncalves, Comparative AFM and TEM investigation of the morphology of Nylon6–rubber blends, Polym. Test. 23 (2004) 231–237.
[11] E. Kester, U. Rabe, L. Presmanes, Ph. Tailhades, W. Arnold, Measurements of Young's modulus of nanocrystalline ferrites with spinel structure by atomic force acoustic microscopy, J. Phys. Chem. Solids 61 (2000) 1275–1284.
[12] U. Rabe, S. Amelio, E. Kester, V. Scherer, S. Hirsekorn, W. Arnold, Quantitative determination of contact stiffness using atomic force acoustic microscopy, Ultrasonics 38 (2000) 430–437.
[13] V. Snitka, A. Ulcinas, V. Mizariene, Characterization of materials' nanomechanical properties by force modulation and phase imaging atomic force microscopy with soft cantilevers, Mater. Character. 48 (2002) 147–152.
[14] D.C. Hurley, A. Kopycinska-Mueller, A.B. Kos, R.H. Geiss, Quantitative elastic property measurements on the nanoscale with atomic force acoustic microscopy, Adv. Eng. Mater. 7 (8) (2005) 713–717.
[15] M. Preghenella, A. Pegoretti, C. Migliaresi, Thermomechanical characterization of fumed silica–epoxy nanocomposites, Polymer 65 (1) (2005) 12065–12072.
[16] B. Russell, R. Chartoff, The influence of cure conditions on the morphology and phase distribution in a rubber-modified epoxy resin using scanning electron microscopy and atomic force microscopy, Polymer 46 (2005) 785–798.
[17] S. Park, W.K. Chung, Y. Youm, J.W. Lee, Natural frequencies and open-loop responses of an elastic beam fixed on a moving cart and carrying an intermediate lumped mass, J. Sound Vib. 230 (2000) 591–615.
[18] K.L. Johnson, Contact Mechanics, Cambridge University Press, Cambridge, 1985.
[19] S. Liu, Q. Wang, Studying contact stress fields caused by surface tractions with a discrete convolution and fast Fourier transform algorithm, J. Tribol. 124 (2002) 36–45.
[20] W.D. Kingery, H.K. Bowen, D.R. Uhlmann, Elasticity, Anelasticity and Strength, second ed, Wiley, New York, 1975.